ADVANCED FUNCTIONAL MATERIALS

Supporting Information

for *Adv. Funct. Mater.,* DOI: 10.1002/adfm.202102797

Two-Dimensional Silicene–Stanene Heterostructures by Epitaxy

Daya Sagar Dhungana, Carlo Grazianetti, Christian Martella, Simona Achilli, Guido Fratesi,* and Alessandro Molle**

Supporting Information

Two-dimensional Silicene-Stanene Heterostructures by Epitaxy

Daya Sagar Dhungana, Carlo Grazianetti*, Christian Martella, Simona Achilli, Guido Fratesi* and Alessandro Molle*

Dr. D. Dhungana, Dr. C. Grazianetti, Dr. C. Martella, Dr. A. Molle
CNR-IMM Agrate Brianza Unit, via C. Olivetti 2, Agrate Brianza, I-20864, Italy
E-mail: carlo.grazianetti@mdm.imm.cnr.it, alessandro.molle@mdm.imm.cnr.it

Dr. S. Achilli, Prof. G. Fratesi
Dipartimento di Fisica "Aldo Pontremoli", Università degli Studi di Milano, via Celoria 16, I-20133 Milano, Italy
E-mail: guido.fratesi@fisica.unimi.it

Keywords: Xenes, Heterostructure, Silicene, Stanene, Molecular Beam Epitaxy

Table of Contents

S1: Collection of LEED images post Sn deposition (Heterostructure type-I, first deposition)

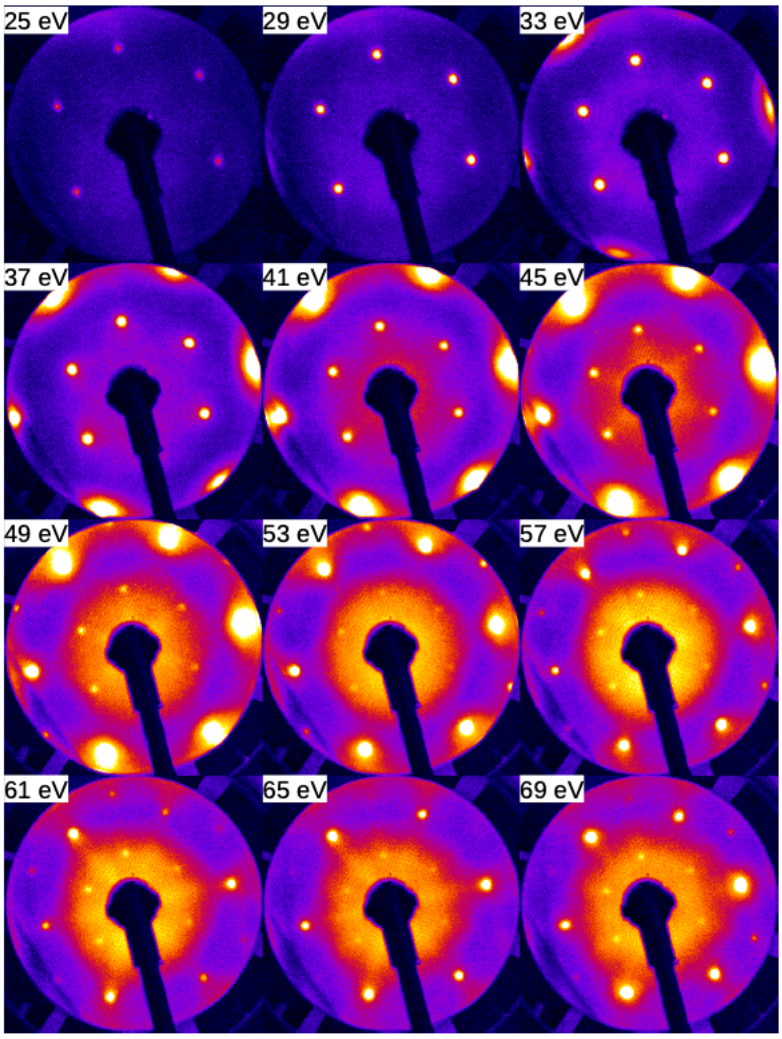

Figure S1: Collection of LEED images for first deposition (Sn) from heterostructure type-I **(figure 1b)** from 25 eV to 69 eV incident LEED energy (E_i). E_i increases by 4 eV when moving from left to right and 12 eV from top to bottom.

S2: Collection of LEED images post Si deposition (Heterostructure type-I, second deposition)

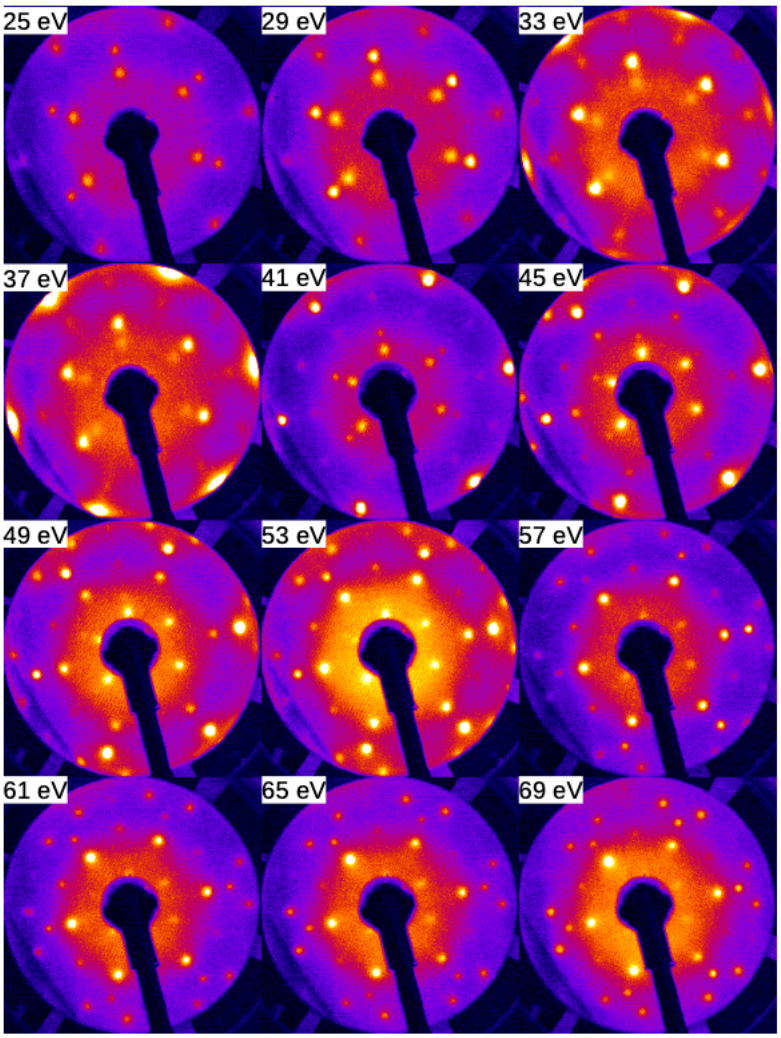

Figure S2: Collection of LEED images for second deposition (Si) from heterostructure type-I **(figure 1c)** from 25 eV to 69 eV incident LEED energy (E_i). E_i increases by 4 eV when moving from left to right and 12 eV from top to bottom.

S3: Collection of LEED images post Si deposition (Heterostructure type-II, first deposition)

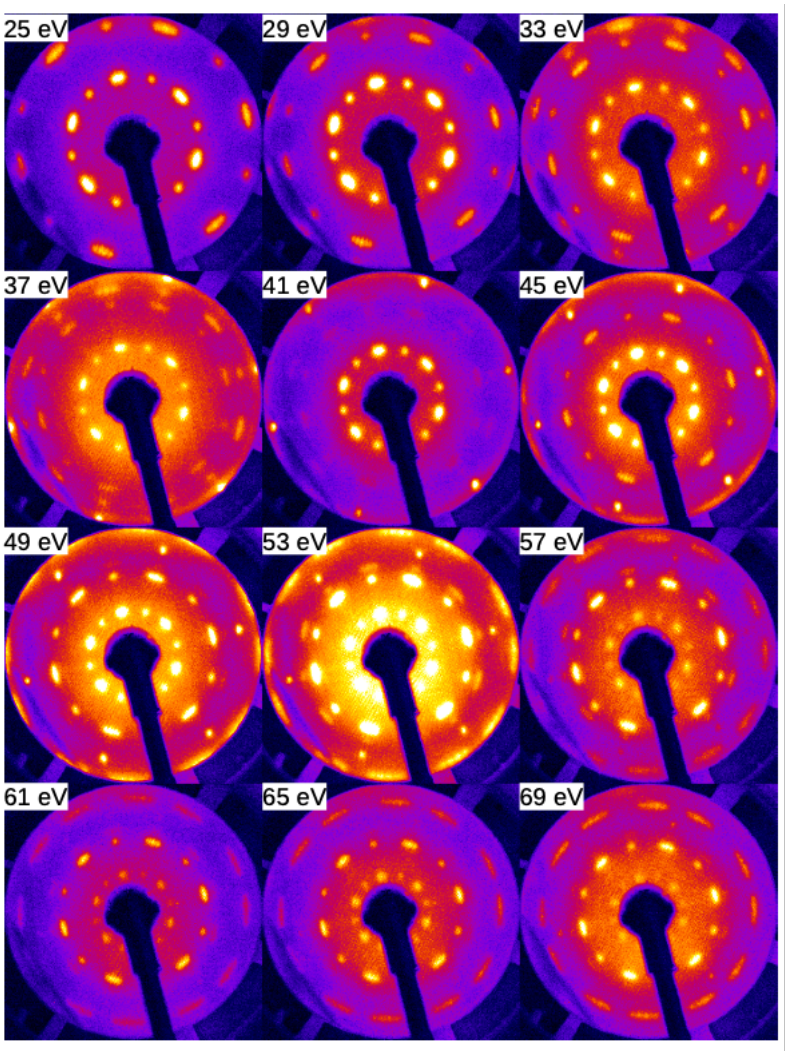

Figure S3: Collection of LEED images for first deposition (Si) from heterostructure type-II **(figure 2b)** from 25 eV to 69 eV incident LEED energy (E_i). E_i increases by 4 eV when moving from left to right and 12 eV from top to bottom.

S4: Collection of LEED images post Sn deposition (Heterostructure type-II, second deposition)

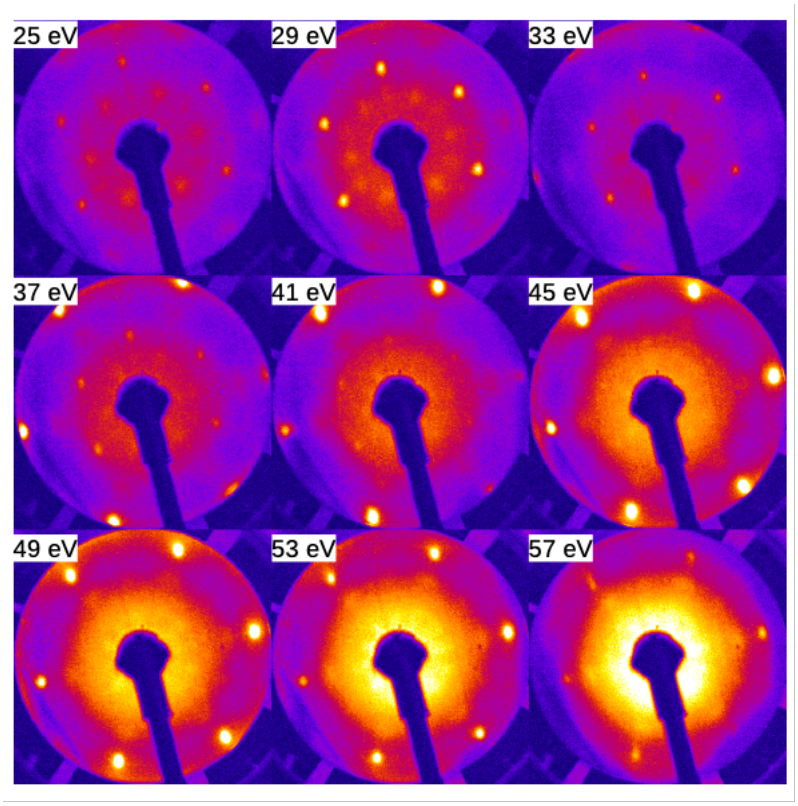

Figure S4: Collection of LEED images for second deposition (Sn) from heterostructure type-II **(figure 2c)** from 25 eV to 57 eV incident LEED energy (E_i). E_i increases by 4 eV when moving from left to right and 12 eV from top to bottom.

S5: Elaboration of Results (Heterostructure type-I)

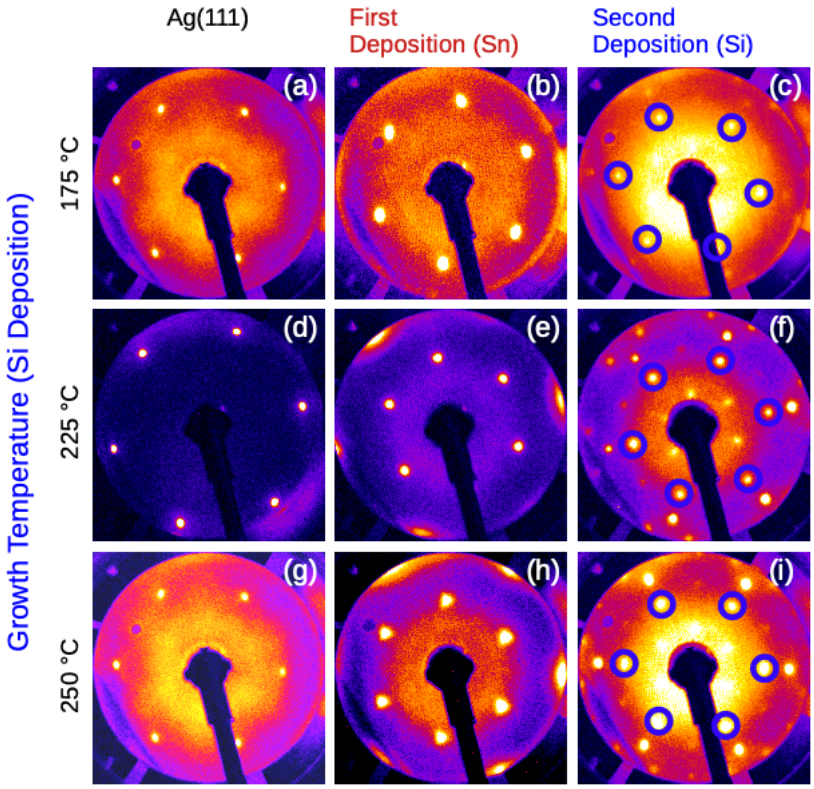

Figure S5: Heterostructure type-I: Silicene on top of Sn:√3x√3 R30°. **(a,d,g)** LEED patterns at incident energy (E_i) = 49 eV on freshly prepared Ag(111) surface with sputtering and subsequent annealing. **(b,e,h)** LEED patterns at E_i = 33 eV observed for Sn: √3x√3 R30° following 1.33 monolayers Sn deposition at 225 °C on top of **(a,d,g)** respectively. **(c,f,i)** LEED patterns acquired following Si deposition on top of Sn:√3x√3 R30° surface **(b,e,h)** respectively at E_i = 52 eV for growth temperatures (175 °C, 225 °C & 250 °C). In all cases, Si:4x4 (blue circles) is observed on top of Sn:√3x√3 R30°. Similarly, the growth temperature hints a possible influence on monolayer formation on the same (or comparable) Sn/stanene surfaces.

S6: Elaboration of Results (Heterostructure type-II)

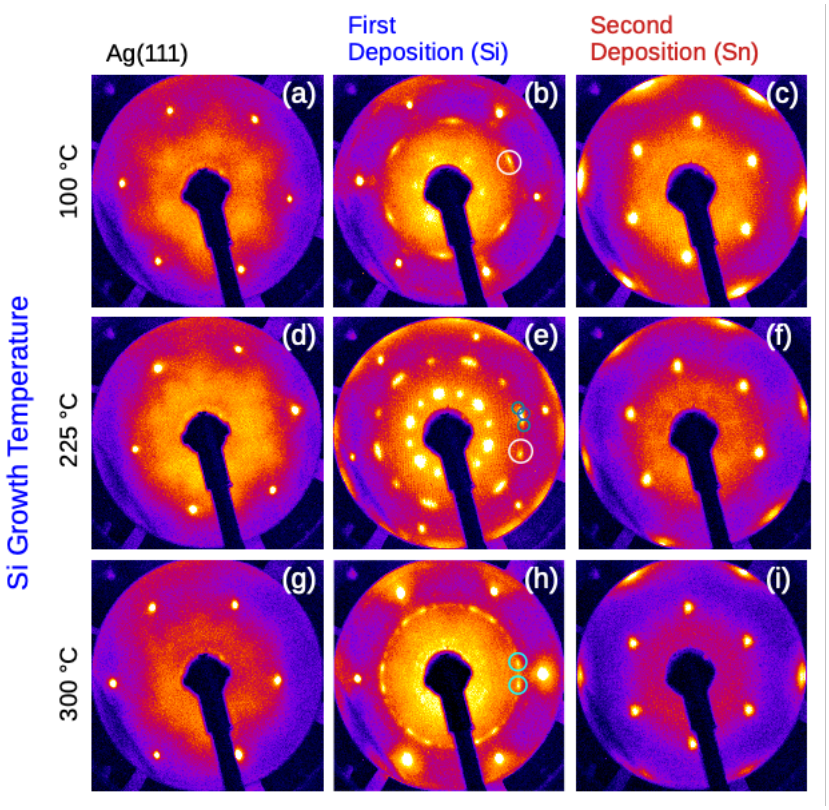

Figure S6: Heterostructure type-II: Sn:√3x√3 R30° on top of various Silicene monolayers. Similar to **figure S5**, **(a,d,g)** are LEED patterns at incident energy (E_i) = 49 eV of Ag(111) surface prepared with sputtering and subsequent annealing. **(b,e,h)** LEED patterns observed (E_i = 52eV, 56eV, 56eV) for silicene monolayers at different growth temperatures: **(b)** 100 °C (post growth annealing implemented; see **S7**), **(e)** 225 °C and **(h)** 300 °C. The silicene phases present are (represented once): **(b)** Si:√13x√13 R13.9° type II (white circle), **(e)** mixed silicene phases: √13x√13 R13.9° type I (green circle), √13x√13 R13.9° type II (white circle), and 4x4 (blue circle), and **(h)** Si:2√3x2√3 R30° (cyan circles). **(c,f,i)** Sn:√3x√3 R30° surface (E_i = 33 eV) is observed following Sn deposition at 225 °C.

S7: Influence of Post-Growth-Annealing for Silicene Monolayer

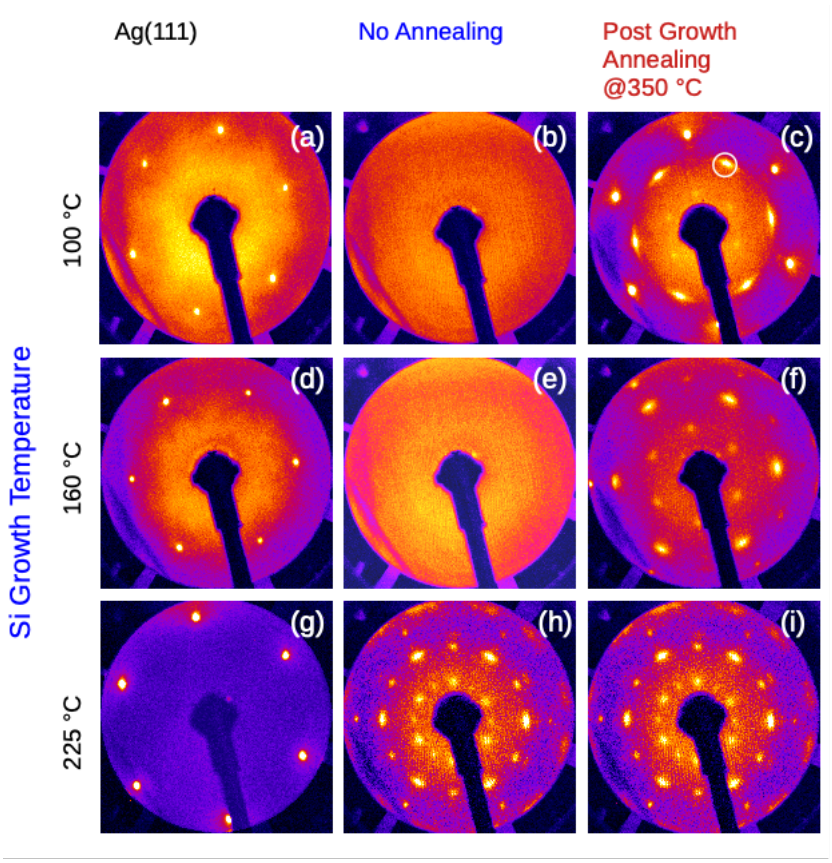

Figure S7: Influence of post-growth-annnealing on epitaxial silicene monolayers. Ag(111) surface LEED patterns **(a,d,g)** before growth and post to surface preparation (sputtering and subsequent annealing). **(b,e,h)** LEED patterns following Si deposition at different temperatures (100 °C, 160 °C, 225 °C). Similarly, **(c,f,i)** respectively present LEED patterns following the 15 minutes post-growth-annealing at 350 °C for **(b,e,h)**. It can be noticed easily that post-growth annealing is helping to obtain the crystalline surface, by transforming the amorphous surface to crystalline, for low temperature growths **(c,f)**. For growth at 100 °C, only √13x√13 R13.9° type II patterns are observed, while when the growth temperature is increased to 160 °C **(f)** two other phases: 4x4 and √13x√13 R13.9° type I are also present in addition. Similarly, all three phases are present when the growth temperature increases to 225 °C **(h & i)** where post growth annealing is showing no effect **(i).** The incident LEED energy (E_i) = 49 eV for **(a,d,g)**, 56 eV for **(f,h,i)** and 52 eV for **(c)**.

S8: LEED mapping

We probe *in situ* LEED as a function of the in-plane position of the sample surfaces. Figure **S8a**, **S8b** and **S8c** respectively present LEED images after preparation, after deposition I and after deposition II for heterostructure type-II. Note that some of the areas can be subjected to high energy electrons during auger acquisition prior to the LEED acquisition. Similar analysis has been performed with ex situ Raman spectroscopic point-scans as a function of the position on the surface therein displaying the same spectrum for each scan considered.

(a) Post Preparation

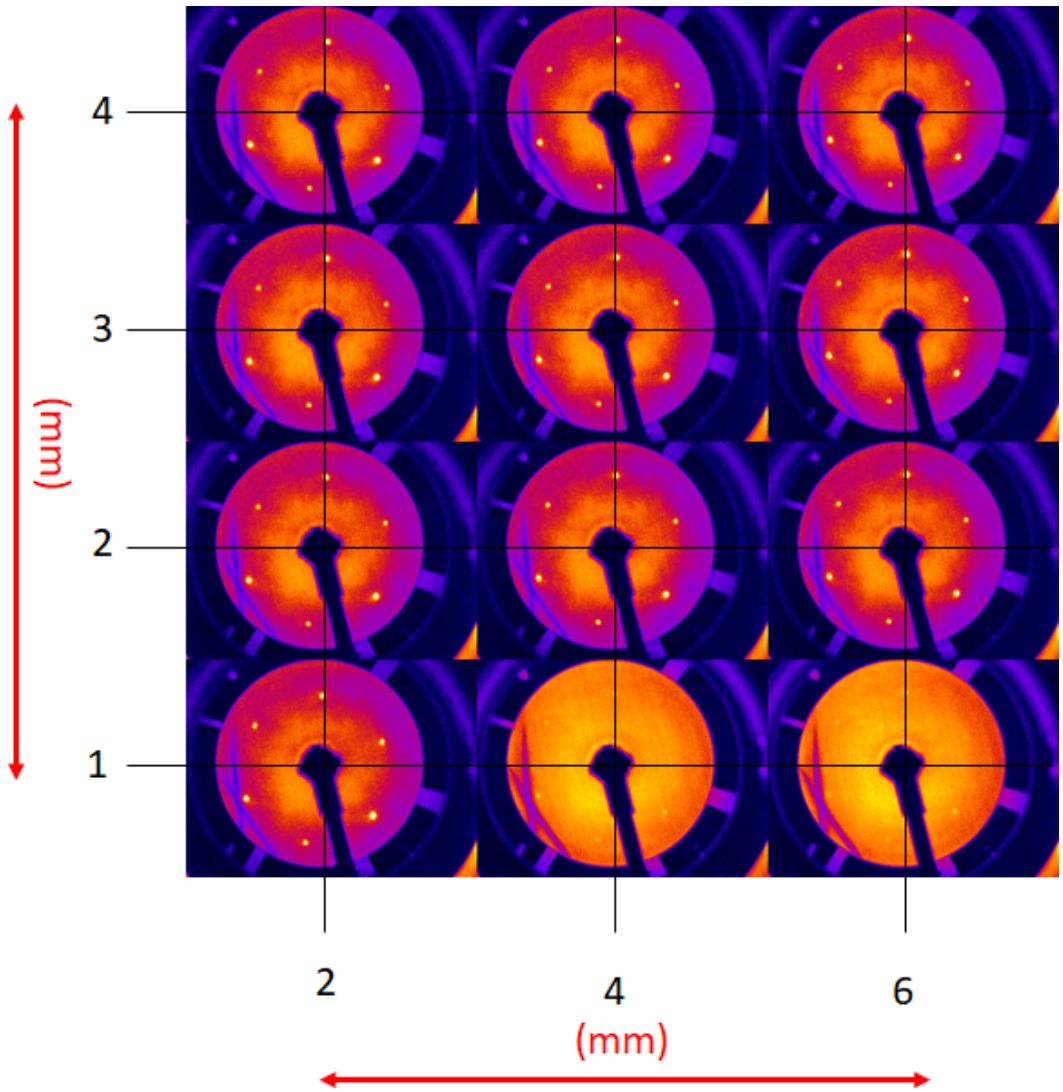

Figure S8a: LEED patterns for several position throughout the surface post to the preparation before any deposition. The incident LEED energy (E_i) is 93 eV. Except the sample in-plane position coordinates, other parameters are unchanged.

(b) Post First Deposition (Si)

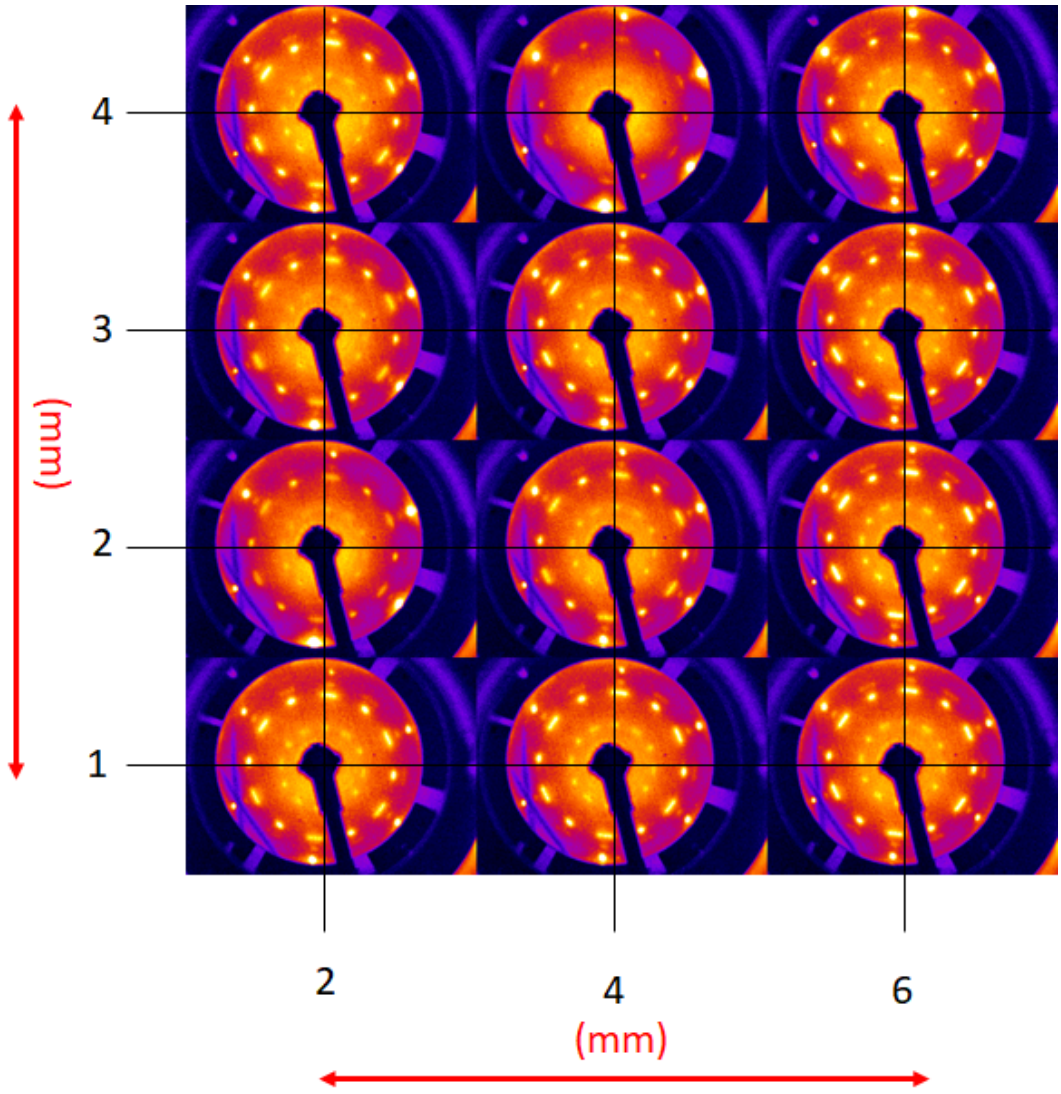

Figure S8b: LEED patterns for several position throughout the surface post to Si deposition on surface shown in **figure S8a** preparation before any deposition. The incident LEED energy (E_i) is 56 eV. Except the sample in-plane position coordinates, other parameters are unchanged.

(c) Post Second Deposition (Sn)

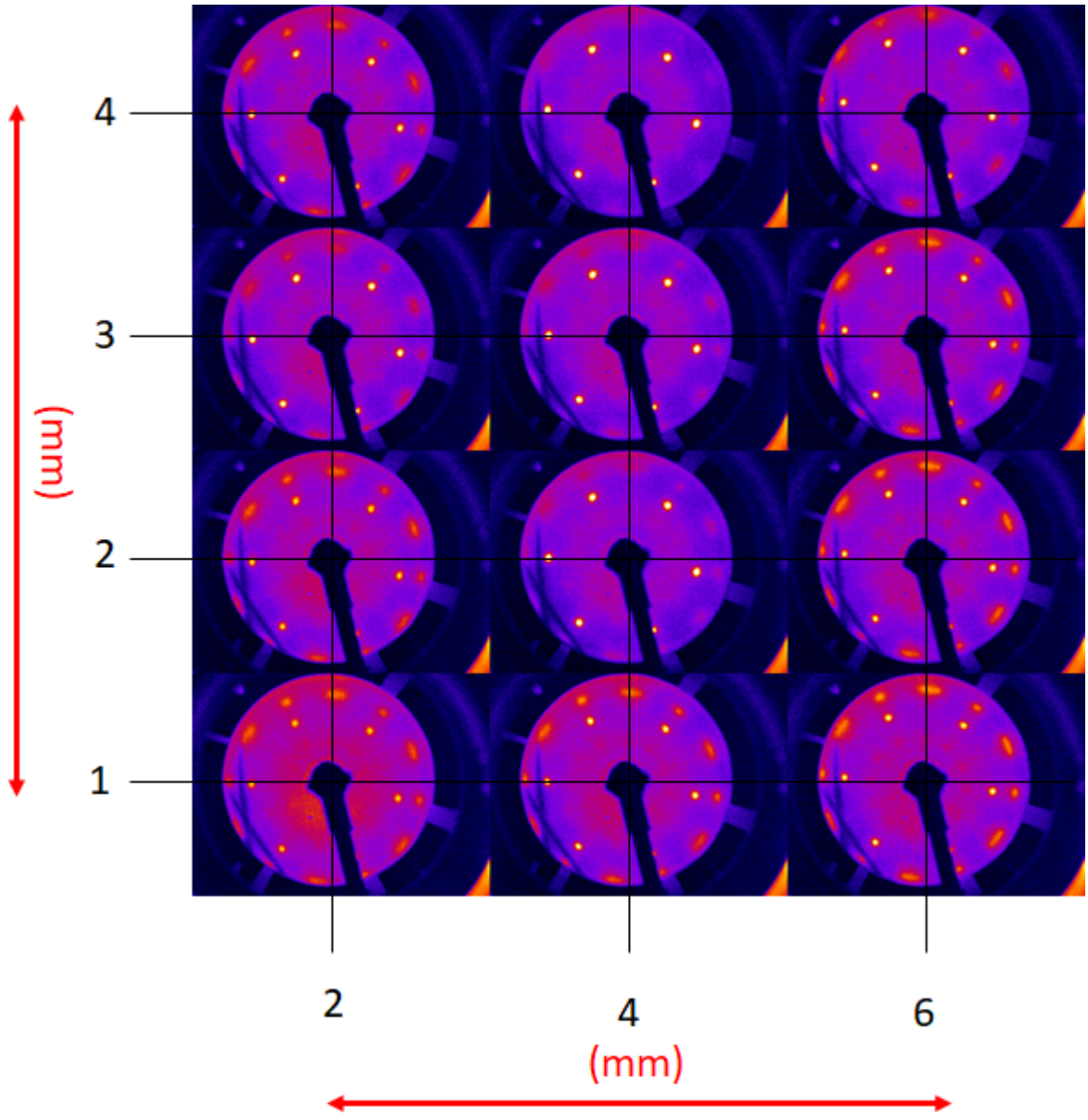

Figure S8c: LEED patterns for several position throughout the surface post to Sn deposition on surface shown in **figure S8b** preparation before any deposition. The incident LEED energy (E_i) is 33eV. Except the sample in-plane position coordinates, other parameters are unchanged.

S9: XPS Analysis (Ag levels)

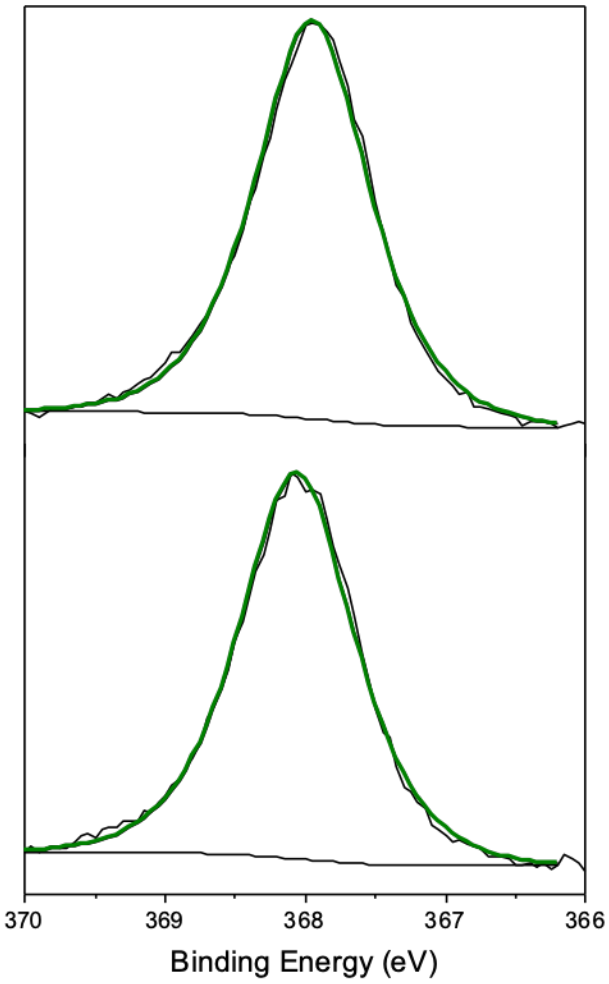

Figure S9: XPS Ag $3d_{5/2}$ core levels of type-I (top) and type-II (bottom) Xenes heterostructures. The binding energy (*Eb*) is 367.94 eV (368.06 eV) with FWHM 0.96 eV (0.97 eV) for type I (type II) heterostructure.

S10: DFT Structural Analysis

To visualize the different heights of the individual Sn and Si atoms in the interfaces, we report in **figure S10** as a color scale the variation of Si (Sn) height with respect to the value averaged over the Si (Sn) overlayer. The buckling of the layers is rather different than that of the individual Xenes on Ag(111). Especially for Sn, we find a significant enhancement of height variations with respect to the nearly flat Sn/$SnAg_2$/Ag(111) case, but also for Si one does not observe the typical patterns of the 4x4 configuration.

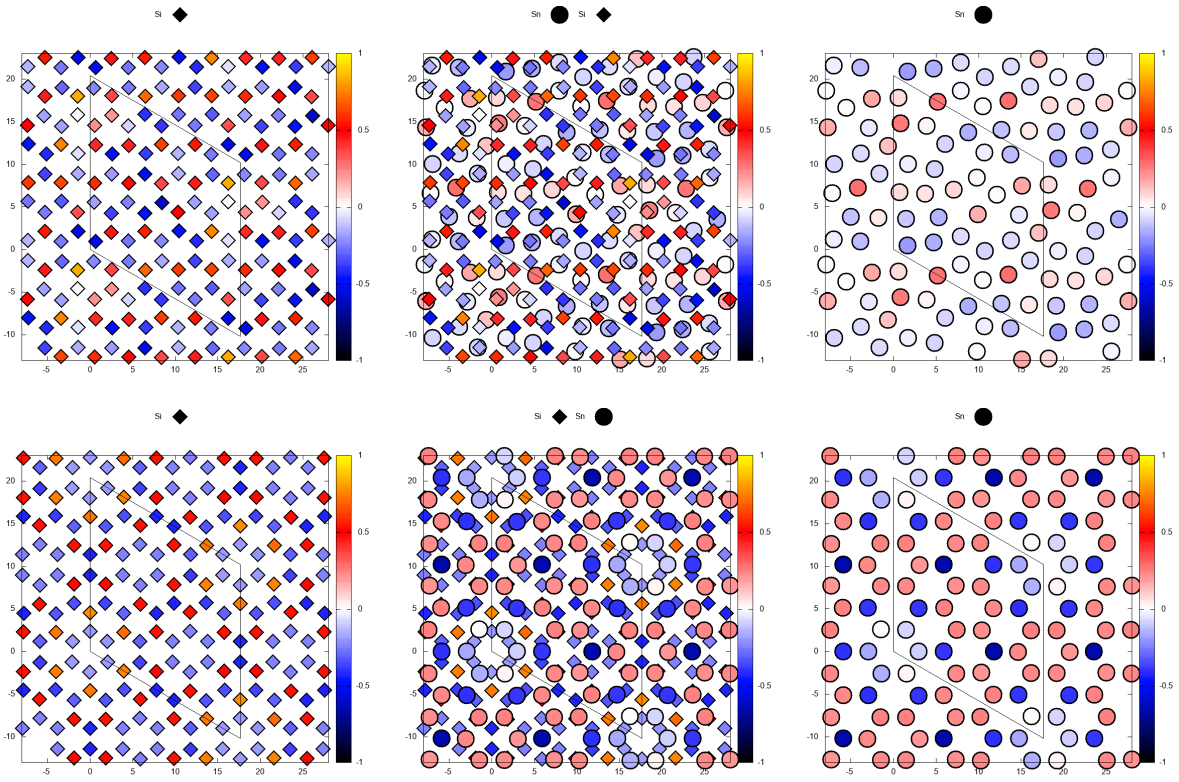

Figure S10: Central panels: top view of the type-I (top panels) and type-II (bottom panels) interface with a color scale representation of the height difference of Si (diamonds) and Sn (circles) atoms with respect to the corresponding average. The left and right panels report separately Si and Sn atoms. The thin line indicates the 4√3x4√3 supercell and Ag atoms are not depicted. Values in Angstrom.

The structural models we analyzed were built from the available experimental input. We recall that a rich phase diagram may be expected (see, e.g., the case of silicene/Ag(111)). For example,

the pristine Sn layer may be displaced over the surface from the Yuhara-like configuration centering the hexagons above tin atoms of $SnAg_2$. This results in an alternative model for type-I heterostructure having very similar properties than the one shown in the main text, and slightly lower energy. As for type-II heterostructure, we note that structural optimizations of models where Sn loses the honeycomb arrangement further lower the system energy, pointing that the model proposed may not be the global minimum for the simulations in the numerical framework adopted. For these structures, however, no experimental evidence is so far provided.

S11: DFT Electronic Properties

Below **Figure S11a** reports on the Density of States of type-I and type-II heterostructures projected onto the atoms of the Sn and Si overlayer (red and blue line, respectively). The PDOS of silicene on Ag in the 4x4 phase and of Sn on Ag having √3x√3 R30° periodicity are also reported for comparison.

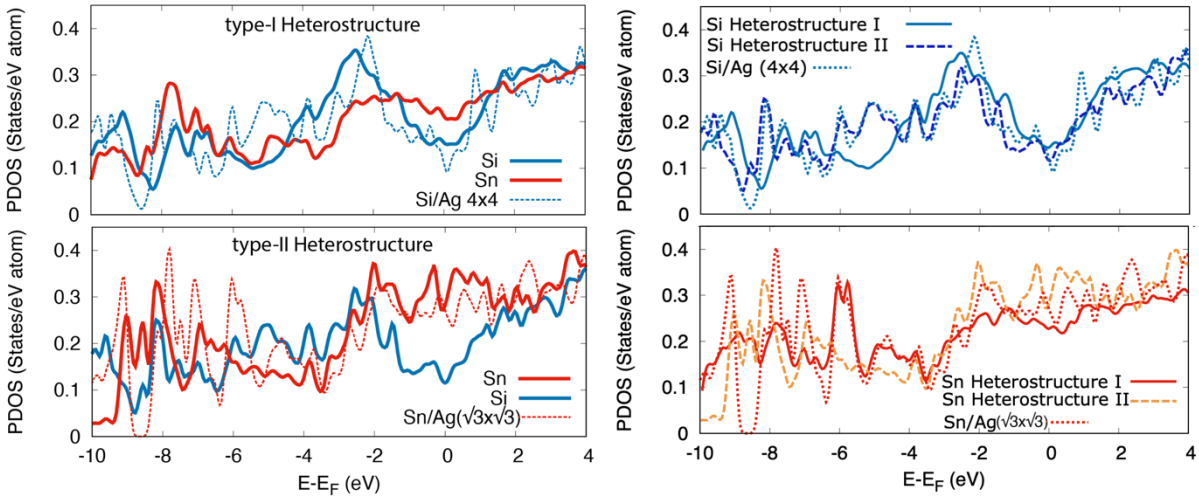

Figure S11a: Projected Density of States (PDOS) of Sn (red) and Si (blue) overlayer in the type-I (top-left panel) and type-II (bottom-left panel) heterostructures. The PDOS of Sn and Si in the pristine Si/Ag and Sn/Ag systems are reported (dashed lines). In the top-right panel the Si PDOS in Heterostructure I (solid blue) and II (dashed ligh blue) has been compared, with reference to Si/Ag(4x4) (dotted). Analogously, in the bottom-righ panel the Sn PDOS in Heterostructure I (solid red) and II (dashed ligh red) is reported in comparison with Sn/Ag(√3x√3) (dotted).

The metallic character of Sn layer in both the heterostructures is evident from the PDOS, as well as the disappearance of the Dirac cone of silicene at the Fermi level, due to the interaction with Ag substrate, as already reported for silicene on Ag[1,2]. The comparison with the pristine Si/Ag and Sn/Ag systems shows a mild change of the electronic properties due to the

introduction of the hetero-layer in between. Moreover, a close similarity is obtained by comparing one species between the two interfaces suggesting that the electronic properties are mildly modified by the Si-Sn interaction and by the relative ordering of the two overlayers.

We now discuss electron density displacements at the interface through inspection of Mülliken charges. Upon adsorption on Ag(111), the silicene layer charges negatively by attracting 0.05e/atom with respect to neutral atoms, whereas stanene on $SnAg_2$/Ag(111) by 0.007e/atom. In the type-I heterostructure, topmost Si has a smaller in magnitude and opposite charge amounting to -0.01e/atom, while Sn is electron rich by 0.02e/atom. In the type-II, sandwiched Si keeps a charge (0.06e/atom) similar to that of pristine silicene/Ag(111), whereas topmost Sn is basically neutral (0.00e/atom). These values result from averages among significantly scattered figures from the individual atoms, as can be seen in **figure S11b** which reports the net electron number (Mulliken number of electrons minus atomic valence) as a color scale.

It is worth noting that there are large fluctuations between the charges at different atoms, according to the local environment and proximity with atoms of the other species. Accordingly, a standard deviation σ=0.03 e/atom for Sn (type I and type II) and σ=0.07 (type I) and 0.04 (type II) for Si can be estimated for the charges reported above.

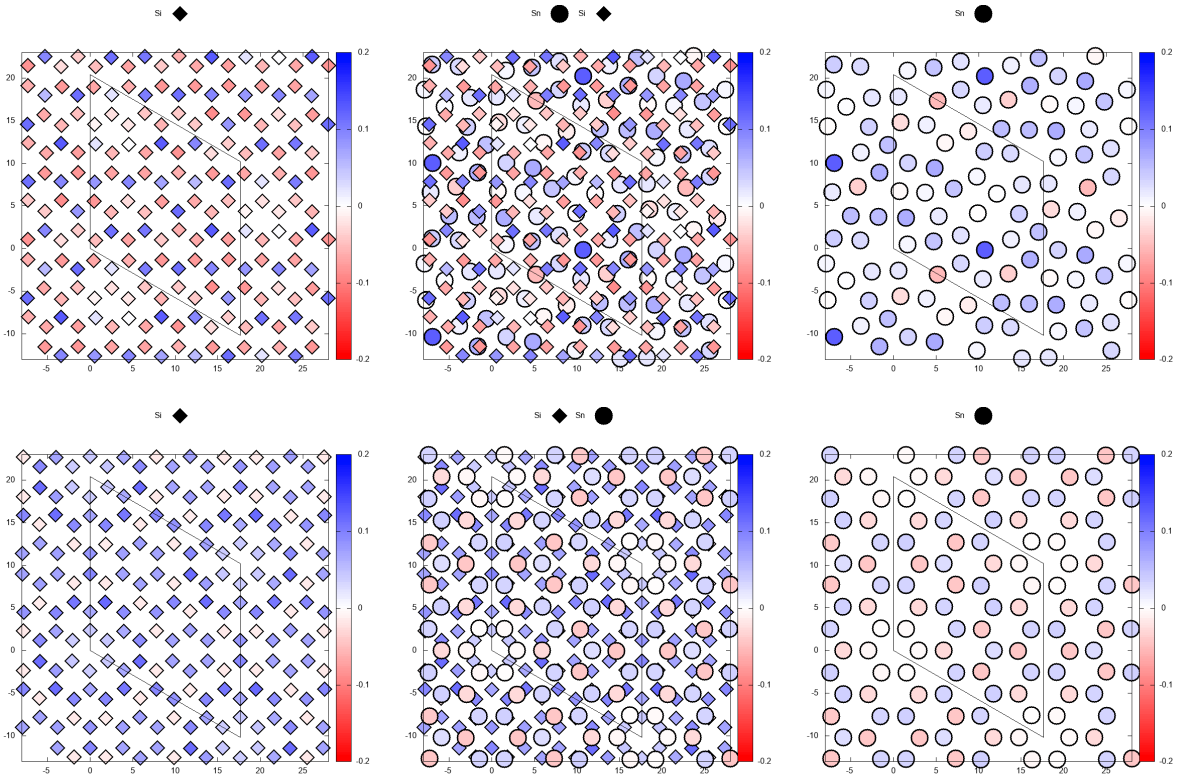

Figure S11b: Central panels: top view of the type-I (top panels) and type-II (bottom panels) interface with a color scale representation of the excess electron number for Si (diamonds) and Sn (circles) atoms. The left and right panels report separately Si and Sn atoms.

T1: Auger peak intensities vs. process stage

Below the Auger intensities of the Si, Ag, and Sn Auger peaks are reported as a function of the process stage for both heterostructure. Si/Sn peaks are referenced to the first Si/Sn deposition stage in the process sequence, Ag peaks are referenced to the freshly prepared substrate (Post Preparation stage). Statistics is based on 5 spectra post to each stage.

Heterostructure Type-I

	Si	Ag	Sn
Post Preparation	0	100	0
Post Sn	0	75	100
Post Si	100	55	50

Heterostructure Type-II

	Si	Ag	Sn
Post Preparation	0	100	0
Post Si	100	83	0
Post Sn	55	65	100

Supporting Information References

[1] P. M. Sheverdyaeva, S. Kr. Mahatha, P. Moras, L. Petaccia, G. Fratesi, G. Onida, C. Carbone, *ACS Nano* **2017**, *11*, 975.

[2] S. K. Mahatha, P. Moras, V. Bellini, P. M. Sheverdyaeva, C. Struzzi, L. Petaccia, C. Carbone, *Physical Review B - Condensed Matter and Materials Physics* **2014**, 89, 201416(R).